Efficient orthonormal aberration coefficient estimation for wavefront sensing over variable non-circular pupils of the Hobby-Eberly Telescope

Lee, Hanshin, Hart, Michael, Hill, Gary, Rafal, Marc

Hanshin Lee, Michael Hart, Gary J. Hill, Marc D. Rafal, "Efficient orthonormal aberration coefficient estimation for wavefront sensing over variable non-circular pupils of the Hobby-Eberly Telescope," Proc. SPIE 7738, Modeling, Systems Engineering, and Project Management for Astronomy IV, 77381L (5 August 2010); doi: 10.1117/12.857140

SPIE.

Event: SPIE Astronomical Telescopes + Instrumentation, 2010, San Diego, California, United States

Efficient orthonormal aberration coefficient estimation for wavefront sensing over variable non-circular pupils of the Hobby-Eberly Telescope*

Hanshin Lee[†a], Michael Hart[b], Gary J. Hill[a], M. D. Rafal[a]

[a] McDonald Observatory, University of Texas at Austin, 1 University Station C1402, Austin, TX 78712-0259, USA
[b] Hart Scientific Consulting International L.L.C., E. Burns St., Tucson, AZ 85711, USA

ABSTRACT

Wavefront sensing (WFS) is one of the key elements for active alignment of the new Wide-Field Corrector (WFC), as it tracks sidereal motion, with respect to the fixed Hobby-Eberly Telescope (HET) primary mirror. During a track, part of the 10m-pupil of the WFC can lie outside the primary periphery and be clipped off. An additional field-dependent central obscuration by the holes and baffles of the WFC leads to complex pupil geometries. The combination of these is a complicated dynamically varying non-circular telescope pupil. This unique problem to the WFS on the HET needs to be dealt with by choosing an appropriate set of orthonormal aberration polynomials during wavefront reconstruction. In this paper, three ways of computing orthonormal aberration polynomials and their coefficients are discussed. These are based on the Gram-Schmidt (GS) process, but differ in the way of computing key integrals during the GS process. The first method analytically computes the integrals, where a computer algebra program is used. The second uses the Gaussian quadrature over triangulated pupil geometries that approximate the true pupil shape. The last uses indirect numerical estimates of the integrals, which turned out to be natural by-products of the usual least-square Zernike polynomials fit. It is shown that the first method is limited to cases of simple pupil shapes, while the second can be applied to more general pupil shapes. However, when dealing with complicated dynamically varying non-circular pupils, the last method can be vastly more efficient than the second and enables the possibility of estimating orthonormal aberration coefficient on the fly. Also noticed is that the last method naturally takes into account the pixelation effect of pupil geometries due to pixel-based imaging sensors (e.g. CCDs). With these benefits, the last method can be used as a viable tool in real-time wavefront analysis over dynamically changing pupils as in the Hobby-Eberly Telescope, which is otherwise vastly inefficient with analytic methods used in past studies.

Keywords: Hobby-Eberly Telescope, Surface figure, Phase Retrieval, Segmented mirror

1. INTRODUCTION

The HET will be upgraded with a 22-arcmin. diameter field of view wide field corrector (WFC), a new tracker and prime focus instrument package (PFIP), and new metrology systems[1]. The new corrector has much improved image quality and a 10 m pupil diameter. The periphery of the field will be used for guiding and wavefront sensing to provide the necessary feedback to keep the telescope correctly aligned. The WFC will give 30 times larger observing area than the current HET corrector. It is a four-mirror design with two concave 1 meter diameter mirrors, one concave 0.9 meter diameter mirror, and one convex 0.23 m diameter mirror. The corrector is designed for feeding optical fibers at f/3.65 to minimize focal ratio degradation, and so the chief ray from all field angles is normal to the focal surface. This is achieved with a concave spherical focal surface centered on the exit pupil. The primary mirror spherical aberration and the off-axis aberrations in the wide field are controllable due to the first two mirrors being near pupils, and the second two mirrors being well separated from pupils. The imaging performance is 0.5 arcseconds or better over the entire 22 arcminute field of view, and vignetting is minimal.

Wavefront sensing (WFS) is one of the key elements for active alignment of the WFC, as it tracks sidereal motion, with respect to the fixed HET primary mirror[2,3]. During a track, part of the 10m-pupil of the WFC can lie outside the primary periphery and be clipped off. An additional field-dependent central obscuration by the holes and baffles of the WFC leads to complex pupil geometries. The combination of these is a complicated dynamically varying non-circular

* The Hobby – Eberly Telescope is operated by McDonald Observatory on behalf of the University of Texas at Austin, the Pennsylvania State University, Stanford University, Ludwig-Maximillians-Universität München,and Georg-August-Universität, Göttingen

† Hanshin Lee.: E-mail: lee@astro.as.utexas.edu

Modeling, Systems Engineering, and Project Management for Astronomy IV,
edited by George Z. Angeli, Philippe Dierickx, Proc. of SPIE Vol. 7738, 77381L
 · doi: 10.1117/12.857140

telescope pupil. This unique problem to the WFS on the HET needs to be dealt with by choosing an appropriate set of orthonormal aberration polynomials during wavefront reconstruction. Zernike polynomials, that constitute one particular orthonormal set over a unit disk, have been applied to various fields[2–4]. However, there are increasingly many optical systems whose pupils are non-circular. In addition, some systems exhibit variability in pupil shape as a function of field and/or pointing angles as the HET. On such pupils, Zernike polynomials loose orthogonality and it is desirable to use the coefficients of new orthonormal aberration polynomials.

Studies show that orthonormal polynomials can be analytically constructed, via the Gram-Schmidt process, for non-circular pupils in simple shape without shape variability, i.e. annulus, hexagon, ellipse and rectangle[7–10]. The studies overlook implementation aspect of the analytic method to wavefront data measured over more complex pixelated pupil shapes (due to pixel-based imaging sensors) with dynamic variability where the ability to obtain orthonormal aberration coefficients can be highly advantageous. Thus potential issues in using the method in such cases are yet to be properly addressed: Though the analytic method can, in principle, be extended to general pupils, as pixelated pupil shape becomes more complex, analytic calculations can be challenging; Any pupil shape change can compound complexity and inefficiency in executing the method in real-time, due to constructing the analytic forms of orthonormal polynomials whenever pupil shape changes.

In this paper, three ways of computing orthonormal aberration polynomials and their coefficients are discussed. The methods use the Gram-Schmidt (GS) process, but differ in the way of computing key integrals during the GS process. The first method analytically computes the integrals, where a computer algebra program is used. The second uses the Gaussian quadrature over triangulated pupil geometry. The last uses indirect estimates of the integrals, which turned out to be natural by-products of the usual least-square Zernike polynomials fit. It is shown that the first method would be limited to simple pupil geometry, while the second can be applied to more general pupil shapes. However, when dealing with complicated variable non-circular pupils, the last method can be vastly more efficient than the second and enables the possibility of estimating orthonormal aberration coefficient on the fly. Also noticed is that the last method naturally takes into account the pixelation effect of pupil geometries due to pixel-based imaging sensors (e.g. CCDs). With these benefits, the last method can be used as a viable tool in real-time wavefront analysis over dynamically changing pupils as in the Hobby-Eberly Telescope, which is otherwise vastly inefficient with analytic methods used in past studies.

2. ORTHONORMAL ABERRATION POLYNOMIALS

2.1 Orthonormal aberration polynomials and the Gram-Schmidt orthonormalization

The Zernike polynomials (Z_i) can be identified by radial and angular orders [n,m][11]. The polynomial index scheme used here follows: Z_i[n1,m1] precedes Z_j[n2,m2] if n1 < n2; if n1 = n2 and |m1| < |m2|, Z_i precedes Z_j ; if n1 = n2, |m1| = |m2|, and m1 < 0, Z_i precedes Z_j . Suppose a wavefront function W(x, y) on a non-circular pupil E that is a subset of a unit disk S. Assume that W can be described in terms of M Zernike polynomials.

$$W = \alpha_1 Z_1 + \alpha_2 Z_2 + \cdots + \alpha_M Z_M = \vec{\alpha}^T \vec{Z} \tag{1}$$

where $\vec{\alpha}$ and $\vec{Z}$ are the column vectors of α_i and Z_i respectively, and T means transpose. The estimation of α_i can be written with A being the area of E as,

$$\sum_{j=1}^{M} \alpha_j F_{ij} = \sum_{j=1}^{M} \alpha_j \iint_E \frac{Z_i Z_j}{A} dA = \iint_E \frac{Z_i W}{A} dA \tag{2}$$

Z_i are not orthonormal over E and thus a M x M matrix F, whose (i, j) element is F_{ij} , is neither unitary nor diagonal. The estimate of α_i can still be given by,

$$\alpha_{i,e} = \sum_{j=1}^{M} G_{ij} \iint_E \frac{Z_i W}{A} dA \tag{3}$$

with G_{ij} being the (i,j) element of $\mathbf{G} = \mathbf{F}^{-1}$. $\alpha_{i,e}$ is neither α_i nor the desired orthonormal aberration coefficient (β_i) of W on E, but closely related to β_i as follows.

It is widely known that new orthonormal polynomials, say U_i, can be determined by the Gram-Schmidt orthonormalization of a known set of orthonormal polynomials (Z_j in our case) [12]. Letting $U_1 = Z_1$, we have

$$V_j = Z_j - \sum_{k=1}^{j-1} C_{jk} U_k, \;\; U_j = V_j \sqrt{A / \iint_E V_j V_j dA} \tag{4}$$

with $C_{jk} = \iint_E Z_j U_k dA / A$ where j = 1, 2, … ,M. Using Eq. 4, the following algebraic relation is obtained.

$$\iint_E \frac{V_i V_j}{A} dA = F_{ij} + \sum_{m=1}^{i-1} \sum_{n=1}^{j-1} C_{im} \delta_{mn} C_{nj} - \sum_{n=1}^{i-1} C_{in} C_{nj} - \sum_{m=1}^{j-1} C_{im} C_{mj} \tag{5}$$

with δmn being the Kronecker delta. Given the orthogonality of Vi, the left hand size of Eq. 5 equals to C_{ii}^2 for I = j or vanishes for $i \neq j$. This reduces Eq. 5 to the following algebraic expressions of the Gram-Schmidt orthonormalization coefficient C_{ij}.

$$C_{ii} = \sqrt{F_{ii} - \sum_{k=1}^{i-1} C_{ik}^2}, \;\; C_{ij} = \frac{F_{ij}}{C_{jj}} - \sum_{k=1}^{j-1} \frac{C_{ik} C_{jk}}{C_{jj}} \tag{6}$$

$C_{i,j}$ is essentially the (i,j) element of a M x M lower triangle matrix **C** which can be obtained from the Cholesky decomposition of F as noted in a different way elsewhere [9]. From Eq. 4, we obviously obtain

$$\vec{Z} = \mathbf{C}\vec{U} \;\; \text{and} \;\; \vec{U} = \mathbf{D}\vec{Z} \tag{7}$$

where **D** is $\mathbf{C}^{-1}$. Multiplying $\vec{\alpha}_e$ (the vector of $\alpha_{i,e}$) to Eq. 7 yields a relation between $\vec{\alpha}_e$ and $\vec{\beta}$, also recognized in [9], as,

$$\overrightarrow{\alpha_e}^T \mathbf{C} = \vec{\beta}^T \;\; \text{and} \;\; \vec{\beta}^T \mathbf{C}^{-1} = \vec{\beta}^T \mathbf{D} = \vec{\alpha}_e^T \tag{8}$$

The above orthonormalization process clearly indicates that knowing **F** is central to computing **C** and constructing analytic forms of $\vec{U}$ which can be fitted to wavefront data to determine $\vec{\beta}$. This analytic derivation of **F** can be done for simple pupil shapes, but it can be non-trivial over a complicated pupil domain even using a computer algebra software[13].

2.2 Semi-analytic approach to computing the integral matrix F

One way of computing **F** is to do the integration over a set of smaller and simpler sub-domains of E and then the sum of these integrals yields the total. The simplest shape for the sub-domain is a triangle and the entire pupil can be represented by a set of triangle elements, for which one may use any 2D triangulation codes. As these codes tend to produce triangles in arbitrary shapes and orientations, it is convenient to compute the integral over a simple triangle (A'B'C') to which the actual triangle (ABC) is transformed. This corresponds to an Affine transform where x and y in ABC are linear functions of u and v in A'B'C' as,

$$\begin{bmatrix} x \\ y \end{bmatrix} = \begin{bmatrix} a & b \\ d & e \end{bmatrix} \begin{bmatrix} u \\ v \end{bmatrix} + \begin{bmatrix} c \\ f \end{bmatrix} \tag{9}$$

One's ABC of choice is subjective and we use the one with A(0,0), B(1,1), and C(1,-1), called the unit triangle. By requiring A,B,C to be transformed to A′,B′,C′, respectively, the Affine coefficients are obtained as follows,

$$a = \frac{x_{B'} - 2x_{A'} + x_{C'}}{2}, \; b = \frac{x_{B'} - x_{C'}}{2}, \; c = x_{A'}, \; d = \frac{y_{B'} - 2y_{A'} + y_{C'}}{2}, \; e = \frac{y_{B'} - y_{C'}}{2}, \; f = y_{A'} \tag{10}$$

$F_{j,k}$ over the i-th triangle is given as,

$$F_{jk}^{(i)} = \frac{J_i}{A} \left\{ \int_0^1 \left(\int_{-u}^{u} Z_j(u,v) Z_k(u,v) dv \right) du \right\} \tag{11}$$

where Ji is the determinant of the Jacobian matrix of Eq. 7 and corresponds to the area of the i-th triangle (thus A = $\sum J_i$). Repeating Eq. 11 for all j,k and summing $F_{jk}^{(1)}$ over I yields F on E. It is certainly possible to obtain the closed-form expression of the integral in terms of the Affine coefficients using a computer algebra system although it becomes more complicated for higher j,k. One can, however, find it more practical to obtain F numerically. As Z_i is a polynomial in x and y that are linear functions of u and v, it is perhaps best to use Gauss-Legendre N-point quadrature for the above integral. With N lager than the half of the sum of the radial orders of Z_j and Z_k, the quadrature can exactly compute the above integral. Equation 11 is re-written as,

$$F_{jk}^{(i)} = \frac{J_i}{A}\left\{\sum_p^N \sum_q^N w_p w_q Z_j(u_p, v_q) Z_k(u_p, v_q)\right\} \tag{12}$$

where w is the Gauss-Legendre weight, $u_p = (t_p + 1)/2$ and $v_q = u_p t_q$ for this ABC with the Gauss-Legendre abscissa t defined within [-1,1]. W and t are computed as described in [R]. The use of a Cartesian coordinate system for the above integral will be appropriate for most cases as the pupil function of an optical system is normally recorded in a 2D rectangular pixel grid. The illuminated pixels represent the actual pupil area and can be extracted to form the geometric boundaries of the pupil, which are then used to produce a triangulated pupil. The wavefront map can be expanded into the new orthonormal polynomials over the grid. If desired, one can use the relationship in Eq. 8 to convert the expansion coefficients into those of other orthonormal aberration polynomials over a different pupil domain.

2.3 Indirect numerical estimation approach to computing the integral matrix F

However, analytically computing F over complex pupil can be out of the question. Although computer algebra software or numerical quadrature could be helpful, it is still required to extract (or approximate) the pupil geometry from a measured pupil illumination and/or to divide the geometry into a number of integrable simpler sub-domains, which would make the whole analytic approach increasingly complicated and vastly inefficient when a large sets of orthonormal polynomials need to be obtained for variable non-circular pupils. In addition, it would be much harder to incorporate the pixelation effect, intrinsic to digital wavefront data, into analytic derivations of **F** and $\vec{U}$, and ultimately into estimating $\vec{\beta}$. Considering that W is recorded on N discrete pixels within E, Eq. 3 can be written in a matrix form as,

$$\vec{W} = \mathbf{Z}\vec{\alpha}_e \rightarrow \hat{\vec{\alpha}}_e = (\mathbf{Z}^T\mathbf{Z})^{-1}\mathbf{Z}^T\vec{W} \approx \vec{\alpha}_e \tag{13}$$

where **Z** is a N x M matrix containing M Zernike polynomials evaluated on the given pixelated pupil (E_{pix}) and $\hat{\vec{\alpha}}_e$ is the estimate of $\vec{\alpha}_e$. Noting that F can be estimated by $\mathbf{F} = (\mathbf{Z}^T\mathbf{Z})/N$, the estimate of $\vec{\beta}$ on E_{pix} is given as,

$$\hat{\vec{\alpha}}_e^T \hat{\mathbf{C}} = \hat{\vec{\beta}}^T \approx \vec{\beta}^T \tag{14}$$

where $\hat{\mathbf{C}}$, the estimate of **C**, is given by using $\hat{\mathbf{F}}$ in Eq. 6. The significant result of Eq. 13 and 14 is threefold: i) all estimated quantities are natural by-products of the least square fit of Zernike polynomials to the discrete wavefront measurement, ii) the estimated coefficients are obtained over the as-measured pixelated pupil geometry but essentially without knowing the functional forms of the orthonormal polynomials over the true pupil E, and iii) the optimality of $\vec{\beta}$ while keeping the simplicity and speed of the usual least-square Zernike fit.

3. EXAMPLES

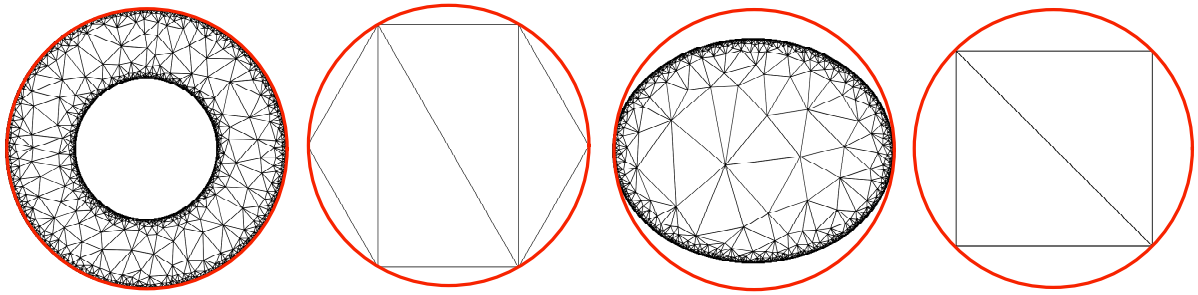

Figure 1. The four pupil shapes used in the comparison of the semi-analytic approach to the analytic method. (From left) Annular, hexagonal, elliptical, and square pupil. Red circles indicate the unit disk over which the Zernike polynomials are orthonormal.

In the first example, we compare the semi-analytic method to the exact analytic method. For this, we use the four pupil shapes as shown in Fig. 1. These pupil shapes are chosen because there exist the analytic expressions of the orthonormal aberration polynomials for these shapes given in Table 2, 6, 12 of Ref. [10]. In the figure, the triangle elements are the

sub-domains for the integration used in the semi-analytic method. The annular and elliptical pupils contain a large number of triangle elements to approximate the curved boundaries, whereas the polygonal pupils (hexagon and square) can be exactly reproduced with only a handful of triangles. The non-zero elements of the conversion matrices (**D** in Eq. 7) of the pupils are given for j, k up to 9 in Table 1.

Table 1. Non-zero elements of **D** given for the four pupils by the semi-analytic method and the existing analytic formulae (i, j up to 9)

Index	**Using the proposed method**				**Using the analytic formulae**			
$D_{i,j}$	Annular	Hexagon	Ellipse	Square	Annular	Hexagon	Ellipse	Square
$D_{01,01}$	1.000000	1.000000	1.000000	1.000000	1.000000	1.000000	1.000000	1.000000
$D_{02,02}$	0.894427	1.095445	1.000000	1.224745	0.894427	1.095445	1.000000	1.224745
$D_{03,03}$	0.894427	1.095445	1.250000	1.224745	0.894427	1.095445	1.250000	1.224745
$D_{04,01}$	-0.577350	0.340997	0.363112	0.790469	-0.577350	0.340997	0.363112	0.790569
$D_{04,04}$	1.333333	1.181249	1.164682	1.369306	1.333333	1.181249	1.164682	1.369306
$D_{05,05}$	0.872872	1.195229	1.250000	1.224745	0.872872	1.195229	1.250000	1.224745
$D_{06,01}$	–	–	-0.473399	1.936492	0.872872	1.195229	-0.473399	1.224745
$D_{06,04}$	–	–	-0.569797	1.936492	0.872872	1.195229	-0.569797	1.224745
$D_{06,06}$	0.872872	1.195229	1.341568	1.936492	0.872872	1.195229	1.341568	1.224745
$D_{07,02}$	-0.146795	0.569383	1.226462	1.234582	-0.146795	0.569383	1.226462	1.234582
$D_{07,07}$	1.037999	1.258171	1.605999	1.454969	1.037999	1.258171	1.605999	1.454969
$D_{08,03}$	-0.146795	0.569383	0.268179	1.234582	-0.146795	0.569383	0.268179	1.234582
$D_{08,08}$	1.037999	1.258171	1.053507	1.454969	1.037999	1.258171	1.053507	1.454969
$D_{09,02}$	–	–	-0.983725	-1.405634	–	–	-0.983725	-1.405634
$D_{09,07}$	–	–	-0.781419	-0.922938	–	–	-0.781419	-0.922938
$D_{09,09}$	0.867722	1.490712	1.520179	2.200852	0.867722	1.490712	1.520179	2.200852

The coefficients by the semi-analytic method match those given by the analytic formulae. The semi-analytic method relies on triangulated pupil geometries. Therefore, polygonal pupils, e.g. hexagon, can be exactly reproduced by few triangles, whereas those with curved boundaries can only be approximated. As a result, polynomials constructed using this approximation naturally differ from those using the exact geometry. Using more and finer triangles along the curved boundaries, but at a cost of computation time, the discrepancy can certainly be reduced. For example, the annular pupil was approximated by 61289 elements and the resultant conversion coefficients differ from those with the exact pupil geometry by $\sim 10^{-8}$. The computation took 4 minutes. With 5642 elements, $\sim 10^{-5}$ of difference was achieved in 80 seconds of computing time. However, the pupil geometry in wavefront analysis is often assumed or estimated by using pupil illumination measurements. The uncertainty in the pupil shape is likely to be dominant over the approximation error due to triangulation.

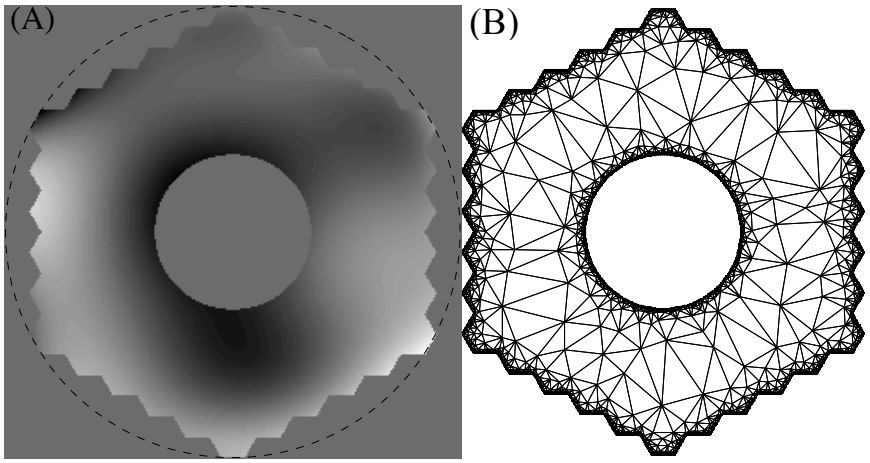

Figure 2. (A) Wavefront map on Pupil A, (B) The triangular integration domains of Pupil A.

In the second example, we compare the numerical estimation method to the semi-analytic approach for a more complicated non-circular pupil. A sample wavefront was constructed over a 256x256 square grid by a set of the first 36 Zernike coefficients that are given from the standard implementation of the Kolmogoroff turbulence model[5] with D/r_0 = 1.4. The synthetic wavefront is filtered through the pupil geometry shown in Fig. 2-(A). The left panel in the figure shows the triangular sub-domains that were used in computing the integral matrix **F** and thus **D** via the semi-analytic integration method described in Section 2.2. The given true Zernike coefficients are converted to the orthonormal aberration coefficients of which the first 15 are listed in "True β_i" columns in Table 2. These listed coefficients are then estimated by fitting the known orthonormal polynomials (given by **D**) to the wavefront. The estimates from this method are listed in the column called "Method X" in Table 2. The orthonormal coefficients are also estimated by using the indirect numerical estimation method as described in Section 2.3. The results from this method are listed in column "Method Y". The difference between the results from two methods is shown in "|X−Y|" column.

Table 2. $\hat{\beta}_i$ by the semi-analytic approach (Method X) and the numerical estimation method (Method Y).

i	True β_i	Method X	Method Y	|X−Y|
1	-0.0076	-0.0076	-0.0072	0.434×10^{-3}
2	-0.1133	-0.1134	-0.1134	0.051×10^{-3}
3	-0.0233	-0.0234	-0.0235	0.055×10^{-3}
4	0.2741	0.2740	0.2741	0.103×10^{-3}
5	-0.0501	-0.0502	-0.0502	0.012×10^{-3}
6	0.1706	0.1706	0.1706	0.023×10^{-3}
7	-0.1108	-0.1110	-0.1107	0.247×10^{-3}
8	-0.0409	-0.0411	-0.0411	0.025×10^{-3}
9	-0.1064	-0.1062	-0.1062	0.070×10^{-3}
10	-0.0369	-0.0365	-0.0365	0.001×10^{-3}
11	-0.0648	-0.0648	-0.0645	0.310×10^{-3}
12	-0.0057	-0.0058	-0.0058	0.063×10^{-3}
13	-0.1070	-0.1071	-0.1072	0.109×10^{-3}
14	-0.0750	-0.0748	-0.0749	0.111×10^{-3}
15	0.0464	0.0466	0.0466	0.018×10^{-3}
σ_W^2	0.1704	0.1703	0.1704	0.034×10^{-3}

Both methods closely approximate the true orthonormal aberration coefficients. The relative difference between the wavefront variances (σ^2) given by two methods is negligible (less than 0.2%) as compared to the true variance on Pupil A. The difference between Method X and Method Y appears to be minimal, in that the relative difference is less than 1% in most cases. In Table 2, we compare some of the elements of **D** given by Method X with those of $\hat{\mathbf{D}}$ by Method Y. Note that i, j up to 11 are used. We omit $\hat{D}_{ij}$ whose absolute values are smaller than the expected estimation error of 0.003. Apparently, Method Y identifies all of the coefficients important for analytically expressing the new polynomials. Also, $\hat{D}_{ij}$ are close to D_{ij} except a few with small contributions. Due to analytically computing **D**, Method X took roughly 72 seconds longer than Method Y did on the same desktop computer. Therefore, the efficiency gain by using Method Y in dealing with dynamically variable non-circular pupils can be immense.

Table 3. Dij by the semi-analytic approach and ˆDij by the numerical estimation method.

i,j	$D_{i,j}$	$\hat{D}_{ij}$	i,j	D_{ij}	$\hat{D}_{ij}$
01,01	1.000	1.000	08,08	1.214	1.214
02,02	1.025	1.025	09,02	-0.006	-0.003
03,03	1.022	1.022	09,07	-0.006	-0.003
04,01	0.109	0.108	09,09	1.068	1.068
04,04	1.355	1.355	10,03	-0.008	-0.011
05,05	1.106	1.106	10,08	-0.007	-0.009
06,01	-0.004	-0.004	10,10	1.385	1.385
06,04	-0.009	-0.008	11,01	0.827	0.827
06,06	1.105	1.104	11,04	0.098	0.096
07,02	0.495	0.493	11,06	-0.007	-0.006
07,07	1.221	1.221	11,11	1.632	1.634
08,03	0.484	0.484	–	–	–

In the last example, another sample wavefront was constructed over a 256x256 square grid by a set of the first 36 Zernike coefficients given by the same atmospheric model as used previously. This synthetic wavefront is then filtered through the pupil geometry shown in Fig. 3. Note carefully that the pupil is not only complex in shape, but also dynamically changes in shape as a function of an arbitrary parameter called "pupil position". This is a typical pupil shape variation of the HET. In this example, we aim to see what difference there is in using orthonormal aberration polynomials instead of Zernike polynomials over non-circular pupils. For this, we use the numerical estimation method for computing the orthonormal aberration coefficients. We use the estimated variance of the wavefront as the comparison metric. That is, the variance of the synthetic wavefront is estimated in three ways: the true variance of the wavefront data (σ^2), the sum of squares of the first 15 of orthonormal aberration coefficients ($\sigma^2(\beta)$), and the sum of squares of the first 15 of Zernike aberration coefficients ($\sigma^2(\alpha)$). These variances are plotted in Fig. 4.

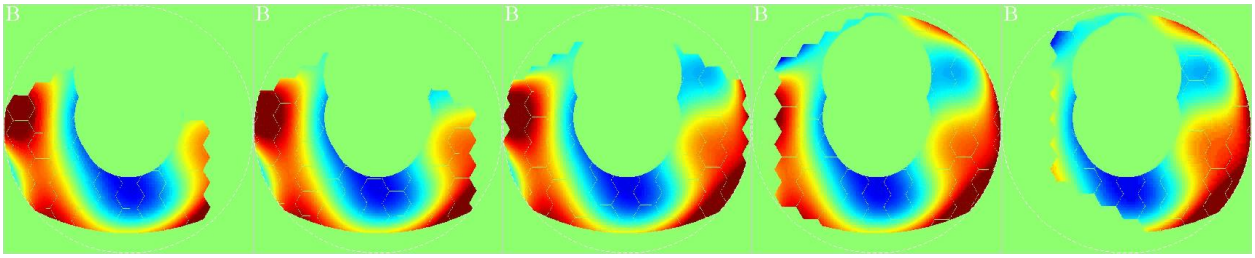

Figure 3. Wavefront map over dynamically varying pupil. From left, the pupil position parameter is 0, 0.3, 0.5, 0.7, 1.

As expected, $\sigma^2(\beta)$ closely approximates σ^2, while $\sigma^2(\alpha)$ differs from the true value significantly. As the pupil shape becomes closer to the unit circle (i.e. pupil position ~ 0.7), $\sigma^2(\alpha)$ asymptotes the other two curves, but quickly diverts away as the pupil shape starts departing from the unit disk again. The last 21 of orthonormal aberration coefficients are also estimated independently and the sum of squares of these ($\Delta\sigma^2(\beta)$) matches the true difference $\Delta\sigma^2 = \sigma^2(\beta) - \sigma^2$.

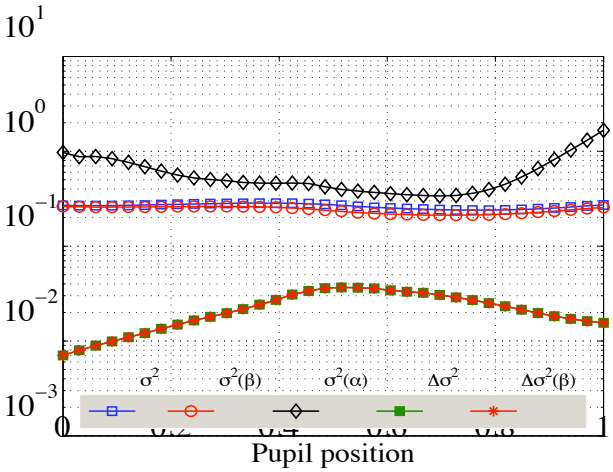

Figure 4.Variance estimates given by different methods.

4. SUMMARY

In this paper, we discussed three different methods of computing orthonormal aberration polynomials over variable non-circular pupils. As demonstrated, all methods are based on the Gram-Schmidt process and can be a useful tool for constructing orthonormal aberration polynomials over non-circular pupils, where the usual Zernike polynomials lose their orthogonality. The fully analytic approach can be replaced by the semi-analytic approach or the numerical estimation method. In the semi-analytic method, the pupil domain is described by simple triangle elements and key integrals of the GS process are performed over these elements via Gaussian Quadrature. Although accurate, its execution speed is substantially compromised. This makes this approach better suit for computing the polynomials over non-circular pupils without shape variability. In comparison to this method, the indirect numerical estimation method shows much faster execution speed with minimal compromise in estimation accuracy. This feature is especially desirable when dealing with complex pupils with dynamic shape variability. It is also shown that this approach can naturally take into account the pixelation effect due to pixel-based imaging sensors used in wavefront sensing. Additionally, it uses the routine least-square fit of Zernike polynomials to wavefront measurements, but without having to know the functional forms of the orthonormal polynomials. This effectively eliminates the time consuming part from the estimation, thereby keeping the simplicity and speed of the usual least-square fit while ensuring the optimality of the resultant orthonormal aberration coefficients over a given pixelated pupil geometry. These features are not only ideal for real-time wavefront analysis over dynamically varying pixelated pupils, but also useful in extending the method to estimating orthonormal slope aberration coefficients, where mean wavefront slope is measured over a further complicated geometry formed by variable noncircular pupils and a coarse slope sampling grid. Currently, we are implementing the last method in wavefront reconstruction using Shack-Hartmann wavefront sensor data. The results from the presented analysis clearly indicates that the last method can be used as a viable tool in real-time wavefront analysis over dynamically changing pupils of the Hobby-Eberly Telescope, which is otherwise vastly inefficient with analytic methods used in past studies. Portions of this paper have been presented in Ref. [14].

ACKNOWLEDGEMENTS

HETDEX is led by the University of Texas at Austin McDonald Observatory and Department of Astronomy with participation from the Universitäts-Sternwarte of the Ludwig-Maximilians-Universität München, the Max-Planck-Institut für Extraterrestriche-Physik (MPE), Astrophysikalisches Institut Potsdam (AIP), Texas A&M University, Pennsylvania State University, and the HET consortium. In addition to Institutional support, HETDEX is funded in part by gifts from Harold C. Simmons, Robert and Annie Graham, The Cynthia and George Mitchell Foundation, Louis and Julia Beecherl, Jim and Charlotte Finley, Bill and Bettye Nowlin, Robert and Fallon Vaughn, Eric Stumberg, and many others, by AFRL under agreement number FA9451-04-2-0355, and by the Texas Norman Hackerman Advanced Research Program under grants 003658-0005-2006 and 003658-0295-2007.

REFERENCES

[1] R. Savage, et al., "Current Status of the Hobby-Eberly Telescope wide field upgrade," Proc. SPIE, **7733**-149 (2010).
[2] H. Lee, et al., "Analysis of active alignment control of the Hobby-Eberly Telescope wide field corrector using Shack-Hartmann wavefront sensors," Proc. SPIE, **7738**-18 (2010).
[3] H. Lee, et al., "Metrology systems for the active alignment control of the Hobby-Eberly Telescope wide-field upgrade," Proc. SPIE, **7739**-28 (2010).
[4] F. Zernike, "Diffraction theory of knife-edge test and its improved form, the phase contrast method," Mon. Not. R. Astron. Soc. **94,** 377 (1934).
[5] N. Roddier, "Atmospheric wavefront simulation using Zernike polynomials," Opt. Eng. **29**, 1174 (1990).
[6] H. Lee, G. B. Dalton, I. A. Tosh, S.-W. Kim, "Computer-guided alignment I : Phase and amplitude modulation of alignment-influenced optical wavefront," Optics Express **15,** 3127 (2007).
[7] C. F. Dunkl, SIAM J., "Orthogonal polynomials on the hexagon," SIAM J. Appl. Math.**47**, 343 (1987).
[8] R. Upton and B. Ellerbroek, "Gram-Schmidt orthogonalization of the Zernike polynomials on apertures of arbitrary shape," Optics Letters **29**, 2840 (2004).
[9] G. Dai and V. Mahajan, "Nonrecursive determination of orthonormal polynomials with matrix formulation," Optics Letters **32**, 74-76 (2007).
[10] V. N. Mahajan and G. Dai, "Orthonormal polynomials in wavefront analysis: analytical solution," Journal of Optical Society of America A. **24**, 2994 (2007).
[11] M. Born and E. Wolf, Principles of Optics, 7th ed. (Oxford, 1999).
[12] G. B. Arfken, H. J. Weber, F. Harris, Mathematical Methods for Physicists, 5th ed. (Academic,2001).
[13] Maxima ver. 5.18.1 (A Computer Algebra System), http://maxima.sourceforge.net/
[14] H. Lee, "Use of Zernike polynomials for efficient estimation of orthonormal aberration coefficients over variable non-circular pupils," Optics Letters (to be published).